Understanding the role of GLUT2 in dysglycemia associated with Fanconi-Bickel syndrome

Sanaa Sharari
Hamad Bin Khalifa University (HBKU)
Basirudeen Kabeer
Sidra Medicine
Idris Mohammed
Hamad Bin Khalifa University (HBKU)
Basma Haris
Sidra Medicine
Igor Pavlovski
Sidra Medicine
Iman Hawari
Hamad Bin Khalifa University (HBKU)
Ajaz Ahmad Bhat
Sidra Medicine
Mohammed Toufiq
Sidra Medicine
Sara Tomei
Sidra Medicine
Rebecca Mathew
Sidra Medicine
Najeeb Syed
Sidra Medicine
Sabah Nisar
Sidra Medicine
Selma Maacha
Sidra Medicine
Jean-Charles Grivel
Sidra Medicine
Damien Chaussabel
Sidra Medicine
Johan Ericsson
Hamad Bin Khalifa University (HBKU)
Khalid Hussain MBChB (khussain@sidra.org)

Sidra Medicine

Research Article

Keywords: Fanconi-Bickel syndrome (FBS), Dysglycemia, Glucose transporter 2 (GLUT2), PBMCs (Peripheral blood mononuclear cells), miRNAs

Posted Date: March 18th, 2022

DOI: https://doi.org/10.21203/rs.3.rs-1401570/v1

Abstract

Fanconi–Bickel Syndrome (FBS) is a rare disorder of carbohydrate metabolism that is characterized by the accumulation of glycogen mainly in the liver. It is inherited in an autosomal recessive manner due to mutations in the *SLC2A2* gene. *SLC2A2* encodes for the glucose transporter GLUT2 and is expressed in tissues that are involved in glucose homeostasis. The molecular mechanisms of dysglycemia in FBS are still not clearly understood. In this study, we report two cases of FBS with classical phenotypes of FBS associated with dysglycemia. Genomic DNA was extracted and analyzed by whole-genome and Sanger sequencing, and patient PBMCs were used for molecular analysis. One patient had an exonic *SLC2A2* mutation (c.1093C > T in exon 9, R365X), while the other patient had a novel intronic *SLC2A2* mutation (c.613-7T>G). Surprisingly, the exonic mutation resulted in the overexpression of dysfunctional GLUT2, resulting in the dysregulated expression of other glucose transporters. The intronic mutation did not affect the coding sequence of GLUT2, its expression, or glucose transport activity. However, it was associated with the expression of miRNAs correlated with type 1 diabetes mellitus, with a particular significant overexpression of hsa-miR-29a-3p implicated in insulin production and secretion. Our findings suggest that *SLC2A2* mutations cause dysglycemia in FBS either by a direct effect on GLUT2 expression and/or activity or, indirectly, by the dysregulated expression of miRNAs implicated in glucose homeostasis.

1. Introduction

Fanconi and Bickel initially reported the clinical features of the eponymous syndrome (FBS) in 1949 [1]. Mutations in GLUT2 were first reported in three FBS patients, including the first patient in 1997 [2]. More than 100 FBS cases with different *SLC2A2* mutations (missense, nonsense, Fs/InDel, intronic, and compound heterozygous) have been reported until now [3–9]. The *SLC2A2* gene encodes for low-affinity facilitated glucose transporter 2 (GLUT2) (SLC2A2-201 ENST00000314251.8) [3, 10]. GLUT2 is expressed in tissues that play a vital role in glucose homeostasis; GLUT2 in the intestine absorbs glucose from the diet and transports it to the blood [11, 12].

GLUT2 in the human liver, is considered to be a bidirectional transporter. It is involved in taking up glucose for storage as glycogen during the feeding state. It also plays a role in releasing glucose generated either by gluconeogenesis or glycogenolysis during fasting [13–15]. Fasting hypoglycemia, postprandial hyperglycemia, and glycogen storage in FBS patients can be explained by a disturbance in glucose transport and metabolism in the liver. In addition, in the kidney, GLUT2 releases the reabsorbed glucose back to the circulation. Previous investigations suggested that GLUT2 dysfunction in the kidney is associated with glycosuria and glycogen storage [16, 17].

Moreover, GLUT2 is highly expressed in rat beta cells but not in humans. Animal studies suggested that GLUT2 in beta cells has a role in glucose uptake and insulin secretion. However, the role of GLUT2 in human beta cells is still unclear due to a lack of studies [6, 18–20]. FBS patients develop different

patterns of dysglycemia with different severity (fasting hypoglycemia, postprandial hyperglycemia, frank diabetes mellitus, transient neonatal diabetes, and gestational diabetes) regardless of the mutation type.

The molecular mechanisms of dysglycemia in FBS are still controversial and not well explained [3]. One recent study selected a group of FBS mutations associated with dysglycemia and expressed the corresponding GLUT2 mutant proteins in HEK293 cells. Cells transfected with mutated constructs showed the same fructose uptake activity as cells transfected with the wild-type GLUT2, except for p.Thr198Lys, which showed a slight decrease in fructose uptake activity [21].

In the current report, we aimed to clearly understand the mechanisms of dysglycemia in two FBS patients by performing functional studies in patient peripheral blood mononuclear cells (PBMCs).

2. Results

2.1. Clinical and genetic information of patients:

Case 1 is a 19-year-old Pakistani female born to consanguineous parents with the classical phenotype of FBS (Fig. 1a). She was born at term by normal vaginal delivery with a weight of 2.2Kg (< 3rd centile). At the age of 2 years, she developed rickets and recurrent fractures (Fig. 1c). On examination, her height was 100 cm (< 5th percentile), and her weight was 23 kg (< 5th percentile) (Fig. 1b).

In addition, the patient developed renal tubular acidosis with aminoaciduria and her biochemical findings showed dysglycemia (fasting hypoglycemia and postprandial hyperglycemia, low levels of C-peptide) (Table 1). Her HbA1c level was high. Thus, she was diagnosed with diabetes mellitus at the age of 17 years. Diabetes mellitus type 1 evaluation was negative for all autoantibodies, and the patient did not have any features of insulin resistance. HbA1c level decreased from 6.4–6.2% upon treatment with insulin and a DPP4-Inhibitor. Moreover, the patient had hepatomegaly (Fig. 1c) with impaired liver function tests (Table 1). The patient receives multiple medications for electrolyte imbalance (sodium bicarbonate, potassium, phosphorous, and vitamin D).

The patient's WGS revealed a novel homozygous mutation c.613-7T > G: IVS5-7T > G in intron 5 of the *SLC2A2* gene (NM_000340.1), and both parents are carriers. The mutation was confirmed by Sanger sequencing of DNA (Fig. 2a). This mutation has not been reported before and is expected to change the splice site of exon 6, causing the addition of two amino acids by reducing the quality of the splice acceptor site in intron 5 and creating a new cryptic splice acceptor site upstream of the natural splice site. However, the patient's cDNA Sanger sequencing revealed no extra nucleotides between exons 5 and 6 (Fig. 2b), which means the mutation did not affect the coding region of GLUT2 protein. Supplementary igure S1 shows the expected unchanged GLUT2 topology for the patient.

Therefore, we aimed to investigate if there is another possible pathogenic mutation in the *SLC2A2* gene or other genes implicated that might impact GLUT2 expression. The whole-genome sequencing data was uploaded in SeqR, and one additional intronic mutation was found in the *SLC2A2* gene c.15 + 816A > C

(predicted to be likely benign) (Supplementary Fig. S2). The VCF file was generated, and only two non-pathogenic mutations (PIK3CD c. 4C > A, a benign variant; and EP300 c. 1169-4T > C, an intronic mutation) out of 60 genes that regulate GLUT2 expression were detected (Supplementary Fig. 3). Furthermore, we filtered all potential damaging exonic and splice mutations in SeqR, and we found 14 genes (*ACTL9 - ATP8B4 - BMPR1B - COL17A1- CRLF1- FAHD2A- GLDC- HAL- MBTPS2 -NTHL1- PRR5L- SIAE- SLIT3- TMOD3*) out of 757 genes; it is noteworthy that none of them are associated with FBS phenotypes.

Case 2 is an 8-year-old Sudanese boy born to consanguineous parents with the classical phenotype of FBS (Fig. 3a). He was born full-term by normal vaginal delivery with a weight of 3.5 kg. Since two years of age, the patient developed dysglycemia (fasting hypoglycemia, postprandial hyperglycemia, and diabetes mellitus). In addition to hypophosphatemia, hypokalemia, and hyponatremia, the biochemical investigations of the patient showed an increase in random glucose levels and a decrease in the levels of C-peptide and insulin (Table 2). The patient's dysglycemia was controlled by diet and the addition of cornstarch. This patient also has hepatomegaly (Fig. 3c), with impaired liver function tests (Table 2).

In addition, the patient developed renal tubular acidosis and rickets (Fig. 3c). His height and weight were 110.30 cm and 21.4 kg, respectively (Fig. 3b). Full pituitary hormonal tests were in the normal range except for the IGF-1 test, which was low (Table 2). GH stimulation test showed growth hormone deficiency upon which GH 0.5 mg daily was prescribed. Also, the patient received multiple medications for his electrolyte imbalance (sodium bicarbonate, potassium, phosphorous, and vitamin D).

The patient's WGS revealed a homozygous mutation (c.1093C > T in exon 9, R365X (NM_000340)) in the *SLC2A2* gene, and both parents are carriers. The mutation was confirmed by Sanger sequencing of DNA (Fig. 4). Supplementary Fig. S4 shows the expected truncated GLUT2 topology for the patient.

Table 1
Summary of biochemical tests for case 1

Investigation	Test value	Normal range
Electrolyte level		
Serum phosphorus (mmol/L)	0.43	0.93–1.64
Serum calcium (mmol/L)	2.15	2.2–2.7
Serum Sodium (mmol/L)	136	134–146
Serum Potassium (mmol/L)	4	3.5-5.0
Liver function test		
Alanine amino transferase (ALT) (IU/L)	56	8–22
Aspartate transaminase (AST) (IU/L)	74	0–30
Alkaline phosphatase (IU/L)	1108	48–95
Blood glucose test		
Fasting glucose (mmol/l)	2.5	3.5–5.5
2 hours glucose tolerance (mmol/l)	28.2	7.8–11.1
C-Peptide (ng/ml)	0.68	0.78–5.19
HbA1c%	6.4	4.8-6.0
Diabetes mellitus Type 1 evaluation (GAD65, ICA„ ZnT8, IAA)	Negative	-
Growth hormone test		
TSH (mIU/L)	3.82	0.4-4.0
Lipid test		
Cholesterol (mmol/l)	6.53	< 5.18
Triglyceride (mmol/l)	1.3	< 1.7
High Density Lipoprotein (HDL-C) (mmol/l)	0.9	> 1.17
Low Density Lipoprotein LDL (mmol/l)	4.72	< 2.6
Kidney test		
BUN (mmol/L)	1.8	1.9–6.7
Creatinine (µmol/l)	35	54–95
Urinalysis	Generalized Aminoaciduria ++, Phosphaturia	

Table 2
Summary of biochemical tests for case 2.

Investigation	Test value	Normal range
Electrolyte level		
Serum phosphorus (mmol/L)	0.79	0.93–1.64
Serum calcium (mmol/L)	2.17	2.2–2.7
Serum Sodium (mmol/L)	135	134–146
Serum Potassium (mmol/L)	3.3	3.5-5.0
Liver function test		
Alanine amino transferase (ALT) (IU/L)	30	8–22
Aspartate transaminase (AST) (IU/L)	40	0–30
Alkaline phosphatase (IU/L)	388	48–95
Blood glucose test		
Fasting glucose (mmol/l)	3.2	3.5–5.5
2 hour post feed glucose (mmol/l)	18.3	3.5–5.5
Insulin (pmol/l)	6	18–48
HbA1c%	5.7	4-5.6
Diabetes mellitus Type 1 evaluation (GAD65, Insulin,, ZnT8, IA-2)	Negative	-
TSH (mIU/L)	1.72	0.4-4.0
IGF-1 (nmol/L)	7.8	8.2–30.8
PTH intact	10.3	2.0- 6.8
Kidney test		
BUN (mmol/L)	3	2.5–7.1
Creatinine (µmol/l)	34	60–110
Urinalysis	Proteinuria (+ 1), Glucosuria (+ 3)	

2.2. GLUT2 expression in PBMCs: Our study is the first to investigate GLUT2 expression in PBMCs. PBMCs were isolated from patients and healthy controls with no family history of dysglycemia using Ficoll. The expression of GLUT2 protein in each cell type of PBMCs was tested using flow cytometry. The gating strategy used for sorting live PBMCs is illustrated in Fig. 5a. GLUT2 expression was minimal in CD4+, CD8+, CD19 + and CD14 + populations in PBMCs extracted from healthy control (no dysglycemia) (Fig. 5b). It is noteworthy that high expression of GLUT2 in CD8 + cells and its expression in CD4+, CD19+,

and CD14 + cells was observed in a healthy control who had recently received a COVID19 vaccine (Fig. 5c). Therefore, these data propose that GLUT2 is expressed in PBMCs and is activated by an immune response. For a better understanding of the molecular mechanisms of dysglycemia in FBS patients, we decided to extract the PBMCs from the patient with the intronic mutation of SLC*2A2* (C. 613-7T > G, IVS 5-7T > G) and from the patient with the exonic mutation of *SLC2A2* (c.1093C > T in exon 9, R365X).

2.3. Expression of GLUT2 in patient and control PBMCs: Protein lysates were prepared and analyzed by Western blotting to determine the expression of GLUT2 protein. There was no difference in GLUT2 expression between the patient with the intronic mutation and the control (Fig. 6a). However, GLUT2 was overexpressed in the patient with the exonic mutation in comparison to the control (Fig. 6b). Two protein bands were visible in the sample obtained from the exonic patient. Two different GLUT2 specific antibodies were used to confirm this results. Although surprising, the presence of full-length GLUT2 in the patient can be explained by the GLUT2 mRNA being differentially spliced in the patient, removing the stop codon. There is also a possibility that some type of translational mechanism is “silencing” the stop codon [22].

2.4. Glucose uptake activity using patient PBMCs: To study the effect of GLUT2 mutations on glucose uptake activity, 10 mM 2-DG was used. Remarkably, the 2-DG uptake was significantly decreased in the patient with the exonic mutation in comparison to the age- and gender-matched control (Fig. 7a). In contrast, only a slight decrease (non-significant) in glucose uptake activity was observed in the patient with the intronic mutation (Fig. 7b).

2.5. Expression of of alternative glucose transporters in patient PBMCs: We investigated the effect of *SLC2A2* mutation on the expression of other glucose transporters. The gene expression patterns of GLUT1 and GLUT3 were assessed using qRT-PCR. We generated equal amounts of cDNA from normalized good quality RNA extracted from patient PBMCs. The patient with the exonic mutation showed an increase in the expression of both GLUT1 and GLUT3 in comparison to the healthy control (Fig. 8a). However, the patient with the intronic mutation showed a decrease in the expression of GLUT1 and GLUT3 (Fig. 8b). These results suggest the presence of a compensatory mechanism for GLUT2 dysfunction in the patient with exonic mutation, manifested by the activation of expression and function of alternative glucose transporters.

2.6. RNA-Seq analysis of patient PBMCs: RNA was extracted for RNA-Seq analysis to investigate the differentially regulated genes (DEGs) and the corresponding molecular pathways in patients as compared to their controls. Both patients had DEGs compared to their controls. However, these expression patterns were not related to dysglycemia phenotypes, except for the upregulation of RETN (resistin) in the patient (db-bl-0008) with the intronic mutation (Fig. 9a), and the upregulation of ENPP1 in the patient (db-bl-1538) with the exonic mutation (Fig. 9c). Both genes are implicated in insulin resistance and type 2 diabetes mellitus. Both patients displayed DEGs in pathways not associated with dysglycemia (Fig. 9b and d). We concluded that the C-terminal portion of GLUT2 is important for its glucose transport activity and that GLUT2 dysfunction is the underlying cause behind dysglycemia in the patient with the exonic

mutation. However, we cannot exclude another possible mechanism responsible for dysglycemia in the patient with the intronic mutation.

2.7. miRNA analysis for the patient with intronic mutation: Since the intronic mutation in *SLC2A2* did not influence the activity of GLUT2, we undertook more investigation to understand the underlying molecular mechanisms of dysglycemia in FBS. We ran Nanostring miRNA panel v3b covering ~ 800 miRNAs in the patient, mother, and aged- and gender-matching healthy controls with no family history of dysglycemia. We noticed a higher degree of correlation between the patient and the gender and age-matched healthy control, rather than between the patient and the mother, suggesting that the miRNA expression profile might be more influenced by the age and gender rather than relatedness (Supplementary Fig. S5). The unsupervised hierarchical clustering revealed 123 miRs expressed specifically in the patient sample (Supplementary Table S2). The function of these miRNAs was interrogated by using Ingenuity Pathway (IPA) analysis software which returned 118 mapped miRs (Fig. 10). Here we report 30 miRNAs with the highest number of counts difference in the patient in comparison to controls (Fig. 11). We found that 14 of them were correlated with T1DM: 10 miRNAs (miR-199a, miR-25-3p, miR-93-5p, miR-19b-3p, miR-107, miR-24-3p. miR-18a-5p, miR-125b-5p, miR-324-5p, miR-331-3p, and hsa-miR-143-3p) were overexpressed in the control as compared to the patient, and 3 miRNAs (miR-144-3p, let-7e-5p, hsa-miR-29a-3p) were significantly overexpressed in the patient in comparison to the control. Molecular networks, including molecules inferred from previous studies, were generated by IPA functional analysis software (Supplementary Fig. S6). The molecular networks were given a score based on the number of molecules represented in the study dataset as compared to the literature. Network 1 (score 33) includes the genes and miRNAs implicated in organismal injury and abnormalities, skeletal and muscular system development and function, and tissue morphology. The miR-144 family integrated into the network 1. Network 2 (score 31) includes insulin and other genes and miRNAs implicated in glomerular injury, inflammatory disease, inflammatory response, and included miR-29 and let-7 families. These results suggest that dysglycemia in the patient with intronic mutation might be associated with the deregulation of miRNAs involved in insulin production and secretion in beta cells.

2.8. Expressions of genes regulated by miR-29a-3b: Using the RNASeq results, we were interested in investigating if miR-29a-3b overexpression affected the expression of genes involved in insulin production and secretion. We found *CAV2, SLC16A1*, *PIK3R1*, and *SLC2A4* were downregulated in the patient in comparison to control.

3. Discussion

FBS patients develop different patterns of dysglycemia, ranging from fasting hypoglycemia, postprandial hyperglycemia, glucose intolerance to diabetes mellitus [3]. Compound heterozygous or homozygous mutations in *SLC2A2* are the only identified gene mutations implicated with FBS. However, the pattern of dysglycemia does not correlate with the mutation type [3]. The mechanisms involved in the development of dysglycemia in FBS patients is not well known. We hypothesized that classic disturbances in GLUT2 structure and/or function is associated with dysglycemia in FBS.

Glucose uptake activity in peripheral blood mononuclear cells (PBMCs) is vital and plays a key role in inflammation and immune response [23–25]. GLUT2 proteins were not expected to be found in blood cells, and they were not present in the plasma using mass spectrometry (https://www.proteinatlas.org/ENSG00000163581-SLC2A2/blood). Fu et al. reported a difference in the expression and immune action of GLUT1, 3 and 5 in resting and activated human macrophages, monocytes, and lymphocytes [26]. In addition, Palmer et al. reported that the expression of GLUT1 is significantly increased in proinflammatory monocytes from HIV + persons in comparison to HIV- controls [27]. A recent study showed a significant increase in the expression of GLUT4 in the PBMCs extracted from athletes compared to sedentary participants [28]. Moreover, Haas et al. proved using a mouse model an increase in the expression level of GLUTs (1,2,3 and 4) in CD4 + cells activated with CXCL100 [29].

We were interested in examining the expression of GLUT2 in human PBMCs to study the impact of *SLC2A2* mutations on glucose uptake activity. We successfully detected for the first time the expression of GLUT2 in human PBMCs using qRT-PCR. Then, we studied the expression of GLUT2 in different cell types of human PBMCs (T lymphocytes (CD4 + and CD8+), B Lymphocytes (CD19+), and monocytes (CD14+)). We found a very low expression of GLUT2 in different cell types of PBMCs extracted from the healthy control (no dysglycemia) (Fig. 5). However, the expression of GLUT2 was upregulated in all activated PBMCs cell types of a healthy control who recently received the COVID19 vaccine.

Based on the results that we have generated from patient's PBMCs, we suggest that the exonic mutation in GLUT2 affects its glucose transport activity and that this explains the dysglycemia observed in this FBS patient. However, it is still unclear if and how the intronic mutation in GLUT2 impacts on glucose metabolism. In an effort to address this question, we used the Nanostring miRNA panel v3b to investigate if the intronic mutation affected the expression of miRNAs correlated with dysglycemia. The molecular analyses showed that the miRNA expression profiles of the patient were more similar to that of the healthy control than to that of the mother (Supplementary Fig. 5). We identified 123 miRNAs that were expressed specifically in the patient, and the subsequent IPA analysis identified 118 mapped miRNAs (Fig. 10). The highest 30 counts of difference in the expression in the patient in comparison to the control were presented, and 14 miRNAs (miR-199a, miR-25-3p, miR-93-5p, miR-19b-3p, miR-107, miR-24-3p. miR-18a-5p, miR-125b-5p, miR-324-5p, miR-331-3p, miR-144-3p, let-7e-5p, hsa-miR-29a-3p, and hsa-miR-143-3p) were correlated with type 1DM (Fig. 11).

Interestingly, we found the expression of hsa-miR-29a-3p was significantly increased in the patient in comparison to the healthy control. Aghaei et al. reviewed the miR-29 family and its association with insulin secretion and identified three separate mechanisms; either by direct targeting of pancreatic p85α or Stx-1a to influence insulin signaling or fusion of insulin granule with the membrane, respectively, or by targeting hepatic p85α to activate gluconeogenesis [30].

Furthermore, one study demonstrated that miR-29a inhibits glucose-stimulated insulin secretion (GSIS) and cell proliferation in MIN6 cells via a negative effect on Cdc42/β-Catenin signaling [31]. It has also been suggested that miR-29a inhibits GSIS by targeting syntaxin-1 and Mct1, as well as insulin signaling

by targeting INSIG1, CAV2, PIK3R1 [32, 33]. Furthermore, Zhou et al. reported that miR-29a is also implicated in insulin resistance by decreasing ATP production, GLUT4 expression, and glucose uptake through targeting PPARδ [34]. Hromadnikova et al. suggested that hsa-miR-29a-3p could play a role in heart disease and diabetes mellitus [35]. In addition, a recent study showed that miR-29 is involved in inflammation and diabetes mellitus through the down regulation of TRAF3 [36]. Interestingly, we found that the expression of *CAV2, SLC16A1, PIK3R1*, and *SLC2A4* were downregulated in the patient carrying the intronic GLUT2 mutation in comparison to control (Fig. 12). TargetScan (prediction of miRNAs target website) predicted an interaction between miR-29a-3b and position 1341–1347 in the human 3'UTR of *SLC2A2* (ENST00000314251.3). However, miRecords did not predict any interaction.

In addition, two other miRNAs, hsa-miR-144-3p and hsa-let-7e-5p, were also significantly increased in the patient in comparison to the healthy control. Shen et al. showed hsa-miR-144-3p is associated with adipogenesis by promoting C/EBPα activity [37]. Demirsoy et al. reported that the expression of hsa-let-7e-5p was significantly downregulated in patients with T2D after receiving metformin therapy [38]. TargetScan proposed an interaction between has-let-7e-5p and position 878–884 in the 3'UTR of *SLC2A2*. However, miRecords did not predict any interaction.

Moreover, we found that another set of 11 miRNAs (miR-199a, miR-25-3p, miR-93-5p, miR-19b-3p, miR-107, miR-24-3p. miR-18a-5p, miR-125b-5p, miR-324-5p, miR-331-3p miR-199a, miR-25-3p, miR-93-5p, miR-19b-3p, miR-107, miR-24-3p. miR-18a-5p, miR-125b-5p, miR-324-5p, miR-331-3p, and hsa-miR-143-3p) were overexpressed in the patient in comparison to the control. Jordan et al. reported that miR-143 impairs the capability of insulin to stimulate AKT activation and glucose homeostasis by downregulation of oxysterol-binding-protein-related protein 8 (ORP8) [39]. Guo et al. reported that the expression of miR-324-5p was elevated in patients with hyperlipidemia and hyperglycemia due to suppression of ROCK1 [40]. Yu et al. reported that overexpression of miR-125b-5p improves the function of pancreatic β-cell through suppression of DACT1 [41]. Tavano et al. reported reported that miR-18a-5p was overexpressed in both pancreatic cancer and non-pancreatic cancer with a recent onset of diabetes in comparison to healthy controls [42]. Xu et al. reported that overexpression of miR-125a-5p enhanced hepatic glucose and lipid metabolism (decreasing lipid and glucose levels and increasing glycogen storage) in type 2 diabetes through inhibition of STAT3 expression [43]. Overall, our miRNA analysis clearly demonstrates that the patient carrying the intronic GLUT2 mutation display a different miRNA profile compared to healthy controls. Interestingly, many of the overexpressed miRNAs have been linked to cardiometabolic disease. However, if and how the mutation in GLUT2 is linked to the dysregulated expression of these miRNAs remains to be explored.

The limitations of this study is that we only studied 2 mutations and thus cannot rule out other possible mechanisms of dysglycemia in FBS patients and further functional analysis are required to prove causality of increase in expression of miR-29a-3p in the patient with intronic *SLC2A2* mutation.

In conclusion, our study confirms that homozygous *SLC2A2* mutations are involved in the development of dysglycemia in FBS either by a direct effect on GLUT2 expression and/or activity or by an indirect effect

on other molecules involved in glucose homeostasis.

4. Materials And Methods

4.1. Patient recruitment and clinical information: This study includes two patients diagnosed with FBS associated with dysglycemia. Patients and their families were recruited at Sidra Medicine, and blood samples were collected to perform genetic analysis and to extract PBMCs. In addition, two healthy controls (age- and gender-matched) were recruited at Sidra Medicine, and blood was withdrawn to extract PBMCs. The biochemical and radiological test results of the patients were collected from the medical information system at Sidra Medicine.

4.2. DNA, miRNA, RNA, and PBMCs Isolation: Genomic DNA was isolated from peripheral blood samples following the manufacture's protocol (QIAamp DNA Blood Maxi Kit, Qiagen). PBMCs were purified using the following optimized protocol: 1) blood was diluted with an equal volume of serum-free RPMI media (with glutamine, penicillin/streptomycin); 2) 2 volumes of diluted blood subsequently added to the side of a Falcon tube containing 1 volume Ficoll-Paque™ PLUS (GE Healthcare); 3) the resulting solution was centrifuged at 2000 rpm for 30 min (acceleration 6, deceleration 0), 4) the PBMCs layer was recovered and washed twice with RPMI medium at 1500 rpm for 10 min (acceleration and deceleration 9); 5) the supernatant was discarded and cell pellet was resuspended in 1 ml RPMI for cells counting. PBMCs were either used immediately for glucose uptake assays or stored at -80°C with QIAzol lysis reagent for later extraction of miRNA and RNA according to the manufacture's protocol (miRNeasy Mini kit, QIAGEN).
4.3. Whole-genome and sanger sequencing: We performed whole-genome sequencing using the Illumina HiSeq platform at 30X coverage. The paired FASTQ files resulting from sequencing contained the nucleotides sequence reads and the quality scores for each read. Quality control on fastq files was performed using fastqc software. Sequence reads were aligned to the hs37d53 reference genome using bwa.kit (v0.7.12), which generated a bam file. Quality control on mapped reads was performed using Picard. The variant calling was performed following GATK (4.1) best practices, and joint calling was performed on samples together. The VCF file was normalized and left-aligned using vt. Functional annotation of the combined VCF files was performed using snpEff. The annotated VCF file was further annotated with Clinvar, Gnomad, Thousand Genome projects Allele frequencies, CADD scores, etc., using vcfanno. Each annotated file was uploaded to the Gemini database using vcf2db utilities, and Gemini was used to perform filtering population allele frequency based variant effect and family-based segregation analysis. DELLY software was used for copy number variations (CNV). Sanger sequencing was used to confirm the mutation in patients and their parents using specific primers (Supplementary Table S1). Snapgene software was used for Sanger sequencing analysis
4.4. Flow cytometry: PBMCs were isolated from peripheral blood by centrifugation, as explained above. The optimized protocol was performed as follows: 1) Preparation of stained samples: 1 million cells were stained in 99 µl Dulbecco's Phosphate Buffered Saline (DPBS) with 1 µl Zombie UV Fixable Viability Dye (for live/dead discrimination) for 15 min in the dark, followed by washing with DPBS at 500xg for 5 min. Cells were incubated with either 10µl of anti-human GLUT2 PE-conjugated mouse IgG2a antibody (R&D SYSTEMS, FAB14148) or with only FMO. An antibody cocktail of 5 µl CD4 (BV 421), 5 µl CD8 (BV 605), 5

µl CD14 (AF 647), and 7 µl CD19 (BV 650) was added to all tubes. Subsequently, Brilliant staining buffer (BD Biosciences) was added to a final staining volume of 100 µl and incubated for 15 min in the dark. Washing was performed with cell-staining buffer by centrifugation at 500 xg for 5 min. The cells were fixed with 4% PFA in PBS, incubated for 20 min in the dark at room temperature and washed once with DPBS, by centrifugation for 5 min at 500 xg. 2) Single stain compensation was performed using UltraComp beads (ThermoFisher) individually incubated with 5 µl of each antibody in the dark for 15 min, washed with DPBS, fixed with 4% PFA, and resuspended in DPBS. 3) A small portion of cells was kept unstained. The data was acquired on a BD FACS Symphony A5 flow cytometer. Data analysis was done using FlowJo Software.

4.5. Western Blot: Protein lysates from the patient and control PBMCs were extracted using RIPA buffer with protease and phosphatase inhibitors to examine the expression of GLUT2 protein. Protein lysates were incubated with Laemmli buffer (4x) at 37 ^{o}C for 30 min. Subsequently, samples were run on 10-wells 4–12% gels (ThermoFisher) using MES buffer at 100 V for 90 min and transferred to nitrocellulose membrane using wet transfer. The membranes were blocked in 5% milk for 2 h and incubated with primary GLUT2 antibody (20436-1-AP (Proteintech), 1:300) overnight, followed by five 5 min washes with TBST. The secondary anti-rabbit antibody was added for 2 h, followed by five 5 min washes with TBST, and developed using SuperSignal™ West Pico PLUS Chemiluminescent Substrate. Images were collected using a ChemiDoc™ MP Imaging system (BIO-RAD). Beta-actin was used as an endogenous control.

4.6. Glucose uptake assay: Patient and control PBMCs were immediately used after extraction from fresh peripheral blood samples in glucose uptake assays. 500,000 cells were starved in glucose-free RPMI medium for 1 h, followed by the addition of 10 µl of 10 mM 2-DG for 1 h. Cells were lysed with extraction buffer at 85 ^{o}C for 40 min. The reaction mixtures were neutralized with a 10 µl neutralizing buffer. The glucose uptake activity was tested as recommended by the manufacturer (Abcam, ab136955), and the absorbance was measured at 412 nm using a microplate reader (Flaoster, Omega).

4.7. qRT-PCR: The expression of other glucose transporters (GLUT1 and GLUT3) in patients and control PBMCs were assessed quantitatively. The RNA was extracted from PBMCs as described above and normalized to 200 ng for cDNA synthesis. 3 µl of cDNA products were added and amplified using a 20 µl reaction of SYBR^{R} Green master mix at primer-specific Tms (Supplementary Table S1). The mRNA levels were measured on a QuantStudioTM 12K Flex SystemBlock 96 well instrument. Each PCR reaction used distilled water instead of cDNA as a negative control. Fluorescent data were acquired during the extension phase. Melting curves were generated at the end of each PCR reaction to verify primer specificities. Samples were run in technical replicates. Gene expression was calculated using the 2^-deltaCt method with GAPDH used as the reference gene.

4.8. RNASeq analysis: The RNA extracted from the samples of the patients and controls were submitted to the Genomics Core at Sidra Medicine for RNA-Seq analysis. Library preparation was performed using the TruSeq Illumina RNA Library Prep kit. Libraries were quantified using the KAPA HiFi Library quantification kit on a Roche LightCycler 480 (Roche, Basel, Switzerland). Cluster generation was performed on a cBot instrument. Samples were sequenced on Illumina HiSeq 4000. Processing of RNASeq data was done using the bcbio rnaseq pipeline (bcbio version 1.2.3). Prior to alignment, a quality check of raw data was done using FastQC version 0.11.9. Alignment was done using STAR (version

2.6.1d) and reads were mapped to the hg38 genome. After alignment, Samtools 1.3 was used to collect metrics on BAM files, which were further used to generate a multiQC report. FeatureCounts (version 2.0.0) was used to estimate the expression counts of each gene. Sample read counts were adjusted for library size and normalized using the Trimmed Mean of M-values (TMM) method using Bioconductor package EdgeR (version 3.34.1). Data were log2 transformed. Fold Change (FC) was calculated between patients and their respective controls using EdgeR. Genes with log2 FC of + 2 and − 2 were used for downstream pathway analysis with Ingenuity Pathway Analysis (version 01-18-05) and the Bioconductor package Complex Heatmap (version 2.8.0). ggplot2 library (version 3.3.5) was used for visualization and plotting. 4.9. miRNA analysis: The total RNA extracted from the patient-1 (db-bl-0008), her mother, and age- and gender-matched control-1 were submitted to the Omics Core at Sidra Medicine for Nanostring miRNA profiling. The Nanostring miRNA panel v3b (including ~ 800 targets) was run on all samples. A total of ~ 150 ng of total RNA was used as input for each of the samples assessed. Sample preparation, ligation, hybridization, detection, and scanning were performed as per the manufacturer's instructions. After hybridization, samples were transferred to the nCounter Prep Station, where excess probes were removed, and samples were aligned and immobilized on the nCounter cartridge. The cartridge was placed on the nCounter Digital Analyzer for data collection. The nSolver data analysis software (version 4.0 NanoString Technologies) was used for the assessment of QC and the normalization of the raw gene expression counts. We used the recommended default parameters for quality control flagging; briefly, flags were generated if samples did not meet the following QC criteria: imaging threshold with FOV registration of at least 75%, binding density between 0.05 and 2.25, positive control, and ligation control linearity with R2 > 0.95, positive control limit of detection 0.5fM, positive control > or = 2 standard deviations above the mean of the negative controls. Data are presented as normalized raw counts. Data was imported on ROSALIND (https://app.rosalind.bio/) and Partek Genomic Suite (Partek, St. Louis, Missouri, US) for secondary downstream analysis. Functional gene network analysis was performed using the Ingenuity Pathway Analysis system (QIAGEN, Hilden, Germany), which transforms large data sets into a group of relevant networks containing direct and indirect relationships between genes based on known interactions in the literature.

Declarations

Competing interests: The authors declare no competing interests. All **methods were performed in accordance with the relevant guidelines and regulations by** the Declaration of Helsinki and approved by the Sidra Institutional Review Board (IRB) Committee for the protection of human subjects, Sidra Medicine. Written informed consent forms were completed by all family members involved in the study.

Data Availability Statement: The RNA-Seq and Nanostring assay data has been deposited in the NCBI GEO (GSE198678).

Acknowledgment: We would like to thank Dr. Rafah Mackeh for helping in Western blot.

Authors Contributions: Manuscript writing: S. S., J.E., K.H. Experimental design: S.S., B.K., A.B., J.E., K.H. Experimental work: S.S., B.K., J.E., I.M., I. P., I.H., A. B., R.M., S. N., S. M., J.G., D.C., K.H. Patient recruitment and data collection: S.S, B.H, K.H. Bioinformatic and miRNA analysis: S.T., M.T., N.S. All authors read and approved the manuscript.

References

1. FANCONI G, BICKEL H. Die chronische Aminoacidurie (Aminosäurediabetes oder nephrotisch-glukosurischer Zwergwuchs) bei der Glykogenose und der Cystinkrankheit. Helv Paediatr Acta. Published online 1949.
2. Santer R, Schneppenheim R, Dombrowski A, Götze H, Steinmann B, Schaub J. Mutations in GLUT2, the gene for the liver-type glucose transporter, in patients with Fanconi-Bickel syndrome. Nat Genet. 1997;17(3):324–326. doi:10.1038/ng1197-324
3. Sharari S, Abou-Alloul M, Hussain K, Khan FA. Fanconi–bickel syndrome: A review of the mechanisms that lead to dysglycaemia. Int J Mol Sci. Published online 2020. doi:10.3390/ijms21176286
4. Xiong L-J, Jiang M-L, Du L-N, Yuan L, Xie X-L. Fanconi-Bickel syndrome in an infant with cytomegalovirus infection: A case report and review of the literature. World J Clin Cases. Published online 2020. doi:10.12998/wjcc.v8.i21.5467
5. Eghbali M, Fatemi KS, Salehpour S, Abiri M, Saei H, Talebi S, Olyaei NA, Yassaee VR, Modarressi MH. Whole-Exome Sequencing Uncovers Novel Causative Variants and Additional Findings in Three Patients Affected by Glycogen Storage Disease Type VI and Fanconi – Bickel Syndrome. *Front Genet*. Published online 2021. doi:10.3389/fgene.2020.601566
6. Musa SA, Ibrahim AA, Hassan SS, Johnson MB, Basheer AT, Arabi AM, Abdullah MA. Fanconi Bickel syndrome: clinical phenotypes and genetics in a cohort of Sudanese children. Int J Pediatr Endocrinol. Published online 2020. doi:10.1186/s13633-020-00091-5
7. Ibrahim MN, Laghari TM, Riaz M, Khoso Z, Khan YN, Yasir M, Hanif MI, Flanagan SE, De Franco E, Raza J. Monogenic diabetes in Pakistani infants and children: Challenges in a resource poor country. J Pediatr Endocrinol Metab. Published online 2021. doi:10.1515/jpem-2020-0669
8. Ustkoyuncu PS, Bastug F, Kiraz A, Erdogan M, Eren E, Yıldız G. Tubulopathy and hepatomegaly in a 2-year-old boy: Answers. *Pediatr Nephrol*. Published online 2021. doi:10.1007/s00467-021-04933-z
9. Scully KJ, Wolfsdorf J, Dedekian M. Acquired growth hormone deficiency in Fanconi-Bickel syndrome. BMJ Case Rep. Published online 2021. doi:10.1136/bcr-2021-246212
10. Kentrup H, Altmüller J, Pfäffle R, Heimann G. Neonatal diabetes mellitus with hypergalactosemia. Eur J Endocrinol. Published online 1999. doi:10.1530/eje.0.1410379
11. Stelmańskan E. The important role of GLUT2 in intestinal sugar transport and absorption. *Postepy Biochem*. Published online 2009.

12. Koepsell H. Glucose transporters in the small intestine in health and disease. Pflugers Arch Eur J Physiol. Published online 2020. doi:10.1007/s00424-020-02439-5
13. Karim S, Adams DH, Lalor PF. Hepatic expression and cellular distribution of the glucose transporter family. World J Gastroenterol. Published online 2012. doi:10.3748/wjg.v18.i46.6771
14. Petersen MC, Vatner DF, Shulman GI. Regulation of hepatic glucose metabolism in health and disease. Nat Rev Endocrinol. Published online 2017. doi:10.1038/nrendo.2017.80
15. Chadt A, Al-Hasani H. Glucose transporters in adipose tissue, liver, and skeletal muscle in metabolic health and disease. Pflugers Arch Eur J Physiol. Published online 2020. doi:10.1007/s00424-020-02417-x
16. de Souza Cordeiro LM, Devisetty N, McDougal D, Peters DJM, Chhabra KH. Renal GLUT2 is Essential in Regulating Systemic Glucose Homeostasis by Glycosuria. J Endocr Soc. Published online 2021. doi:10.1210/jendso/bvab048.661
17. Aleksandra S. Human Glucose Transporters in Renal Glucose Homeostasis. Published online 2021.
18. McCulloch LJ, van de Bunt M, Braun M, Frayn KN, Clark A, Gloyn AL. GLUT2 (SLC2A2) is not the principal glucose transporter in human pancreatic beta cells: Implications for understanding genetic association signals at this locus. Mol Genet Metab. 2011;104(4):648–653. doi:10.1016/j.ymgme.2011.08.026
19. De Vos A, Heimberg H, Quartier E, Huypens P, Bouwens L, Pipeleers D, Schuit F. Human and rat beta cells differ in glucose transporter but not in glucokinase gene expression. J Clin Invest. 1995;96(5):2489–2495. doi:10.1172/JCI118308
20. Berger C, Zdzieblo D. Glucose transporters in pancreatic islets. *Pflugers Arch Eur J Physiol*. Published online 2020. doi:10.1007/s00424-020-02383-4
21. Enogieru OJ, Ung PMU, Yee SW, Schlessinger A, Giacomini KM. Functional and structural analysis of rare SLC2A2 variants associated with Fanconi-Bickel syndrome and metabolic traits. Hum Mutat. Published online 2019. doi:10.1002/humu.23758
22. Wangen JR, Green R. Stop codon context influences genome-wide stimulation of termination codon readthrough by aminoglycosides. Elife. Published online 2020. doi:10.7554/eLife.52611
23. Calder PC, Dimitriadis G, Newsholme P. Glucose metabolism in lymphoid and inflammatory cells and tissues. Curr Opin Clin Nutr Metab Care. Published online 2007. doi:10.1097/MCO.0b013e3281e72ad4
24. O'Boyle NJ, Contreras GA, Mattmiller SA, Sordillo LM. Changes in glucose transporter expression in monocytes of periparturient dairy cows. J Dairy Sci. Published online 2012. doi:10.3168/jds.2012-5327
25. Von Ah Morano AE, Dorneles GP, Peres A, Lira FS. The role of glucose homeostasis on immune function in response to exercise: The impact of low or higher energetic conditions. J Cell Physiol. Published online 2020. doi:10.1002/jcp.29228
26. Fu Y, Maianu L, Melbert BR, Garvey WT. Facilitative glucose transporter gene expression in human lymphocytes, monocytes, and macrophages: A role for GLUT isoforms 1, 3, and 5 in the immune

response and foam cell formation. Blood Cells, Mol Dis. Published online 2004. doi:10.1016/j.bcmd.2003.09.002

27. Palmer CS, Anzinger JJ, Zhou J, Gouillou M, Landay A, Jaworowski A, McCune JM, Crowe SM. Glucose Transporter 1–Expressing Proinflammatory Monocytes Are Elevated in Combination Antiretroviral Therapy–Treated and Untreated HIV + Subjects. J Immunol. Published online 2014. doi:10.4049/jimmunol.1303092
28. Sticka KD, Schnurr TM, Jerome SP, Dajles A, Reynolds AJ, Duffy LK, Knall CM, Dunlap KL. Exercise Increases Glucose Transporter-4 Levels on Peripheral Blood Mononuclear Cells. *Med Sci Sports Exerc*. Published online 2018. doi:10.1249/MSS.0000000000001528
29. Haas R, Smith J, Rocher-Ros V, Nadkarni S, Montero-Melendez T, D'Acquisto F, Bland EJ, Bombardieri M, Pitzalis C, Perretti M, Marelli-Berg FM, Mauro C. Lactate regulates metabolic and proinflammatory circuits in control of T cell migration and effector functions. PLoS Biol. Published online 2015. doi:10.1371/journal.pbio.1002202
30. Aghaei M, Khodadadian A, Elham KN, Nazari M, Babakhanzadeh E. Major miRNA involved in insulin secretion and production in beta-cells. *Int J Gen Med*. Published online 2020. doi:10.2147/IJGM.S249011
31. Duan J, Qian XL, Li J, Xiao XH, Lu XT, Lv LC, Huang QY, Ding W, Zhang HY, Xiong LX, Biagio A. MIR-29a negatively affects glucose-stimulated insulin secretion and MIN6 cell proliferation via Cdc42/β-catenin signaling. Int J Endocrinol. Published online 2019. doi:10.1155/2019/5219782
32. Filios SR, Shalev A. β-cell microRNAs: Small but powerful. *Diabetes*. Published online 2015. doi:10.2337/db15-0831
33. Deng J, Guo F. MicroRNAs and type 2 diabetes. ExRNA. Published online 2019. doi:10.1186/s41544-019-0038-5
34. Zhou Y, Gu P, Shi W, Li J, Hao Q, Cao X, Lu Q, Zeng Y. MicroRNA-29a induces insulin resistance by targeting PPARδ in skeletal muscle cells. *Int J Mol Med*. Published online 2016. doi:10.3892/ijmm.2016.2499
35. Hromadnikova I, Kotlabova K, Dvorakova L, Krofta L, Sirc J. Substantially Altered Expression Profile of Diabetes/Cardiovascular/Cerebrovascular Disease Associated microRNAs in Children Descending from Pregnancy Complicated by Gestational Diabetes Mellitus-One of Several Possible Reasons for an Increased Cardiovasc. *Cells*. Published online 2020. doi:10.3390/cells9061557
36. Sun Y, Zhou Y, Shi Y, Zhang Y, Liu K, Liang R, Sun P, Chang X, Tang W, Zhang Y, Li J, Wang S, Zhu Y, Han X. Expression of miRNA-29 in Pancreatic β Cells Promotes Inflammation and Diabetes via TRAF3. Cell Rep. Published online 2021. doi:10.1016/j.celrep.2020.108576
37. Shen L, Li Q, Wang J, Zhao Y, Niu L, Bai L, Shuai S, Li X, Zhang S, Zhu L. miR-144-3p Promotes Adipogenesis Through Releasing C/EBPα From Klf3 and CtBP2. *Front Genet*. Published online 2018. doi:10.3389/fgene.2018.00677
38. Demirsoy IH, Ertural DY, Balci Ş, Çlnklr Ü, Sezer K, Tamer L, Aras N. Profiles of Circulating miRNAs Following Metformin Treatment in Patients with Type 2 Diabetes. *J Med Biochem*. Published online

2018. doi:10.2478/jomb-2018-0009

39. Jordan SD, Krüger M, Willmes DM, Redemann N, Wunderlich FT, Brönneke HS, Merkwirth C, Kashkar H, Olkkonen VM, Böttger T, Braun T, Seibler J, Brüning JC. Obesity-induced overexpression of miRNA-143 inhibits insulin-stimulated AKT activation and impairs glucose metabolism. Nat Cell Biol. Published online 2011. doi:10.1038/ncb2211
40. Guo J, Yang C, Lin Y, Hu G, Wei J, Zhang X, Chen X, Li J. Enhanced peripheral blood miR-324-5p is associated with the risk of metabolic syndrome by suppressing ROCK1. *Biochim Biophys Acta - Mol Cell Biol Lipids*. Published online 2020. doi:10.1016/j.bbalip.2020.158727
41. Yu CY, Yang CY, Rui ZL. MicroRNA-125b-5p improves pancreatic β-cell function through inhibiting JNK signaling pathway by targeting DACT1 in mice with type 2 diabetes mellitus. Life Sci. Published online 2019. doi:10.1016/j.lfs.2019.01.031
42. Tavano F, Fontana A, Mazza T, Gioffreda D, Biagini T, Palumbo O, Carella M, Andriulli A. Early-Onset Diabetes as Risk Factor for Pancreatic Cancer: miRNA Expression Profiling in Plasma Uncovers a Role for miR-20b-5p, miR-29a, and miR-18a-5p in Diabetes of Recent Diagnosis. *Front Oncol*. Published online 2020. doi:10.3389/fonc.2020.01567
43. Xu L, Li Y, Yin L, Qi Y, Sun H, Sun P, Xu M, Tang Z, Peng J. miR-125a-5p ameliorates hepatic glycolipid metabolism disorder in type 2 diabetes mellitus through targeting of STAT3. *Theranostics*. Published online 2018. doi:10.7150/thno.27425

Figures

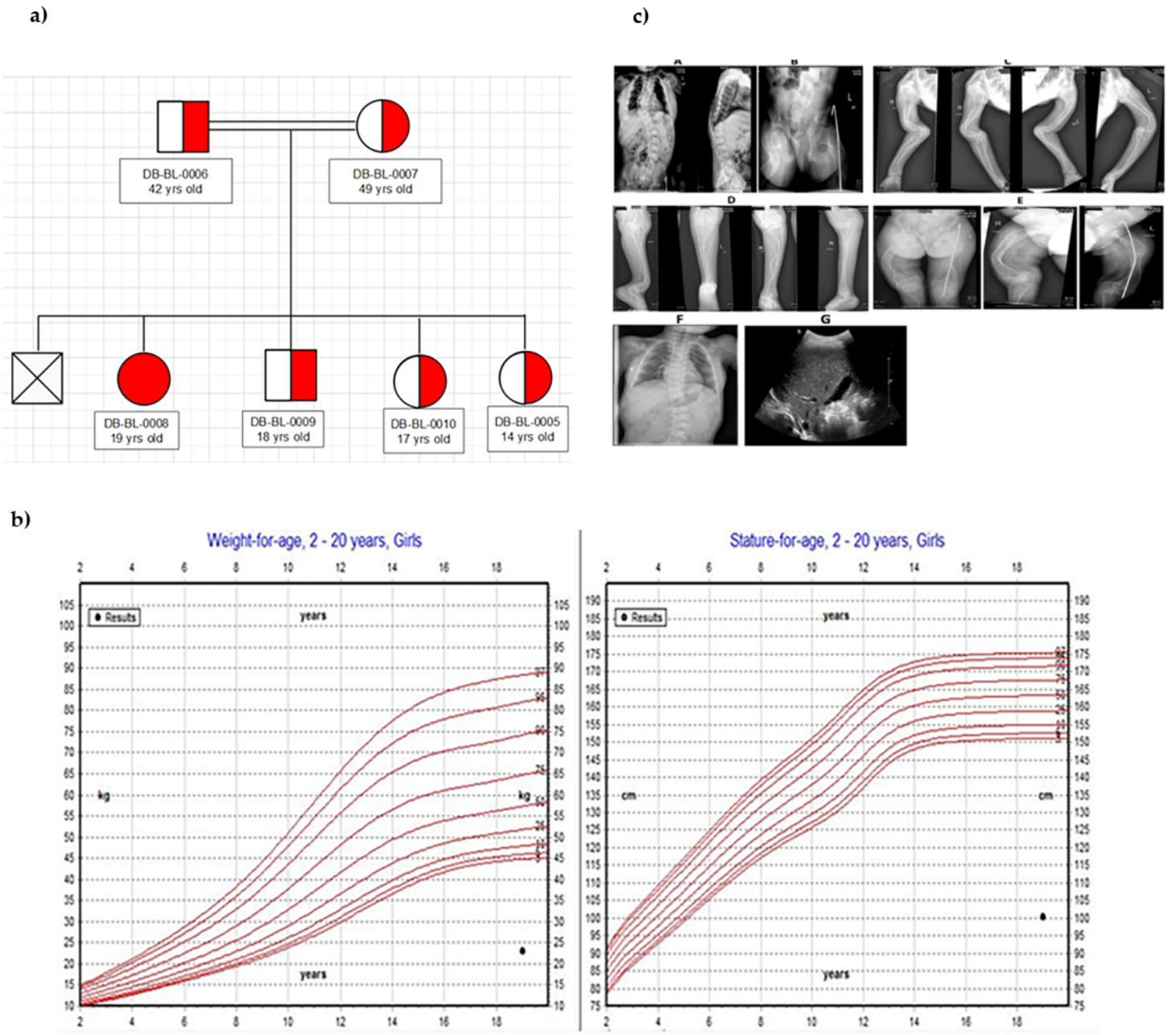

Figure 1

Clinical characteristics of case 1: (a) Family pedigree (patient descend from first-degree cousins). (b) Growth charts. According to WHO length chart: a patient has short stature (dot) and underweight (dot). (c) Radiological findings (rickets and bone deformities (A-F), and hepatomegaly (G)).

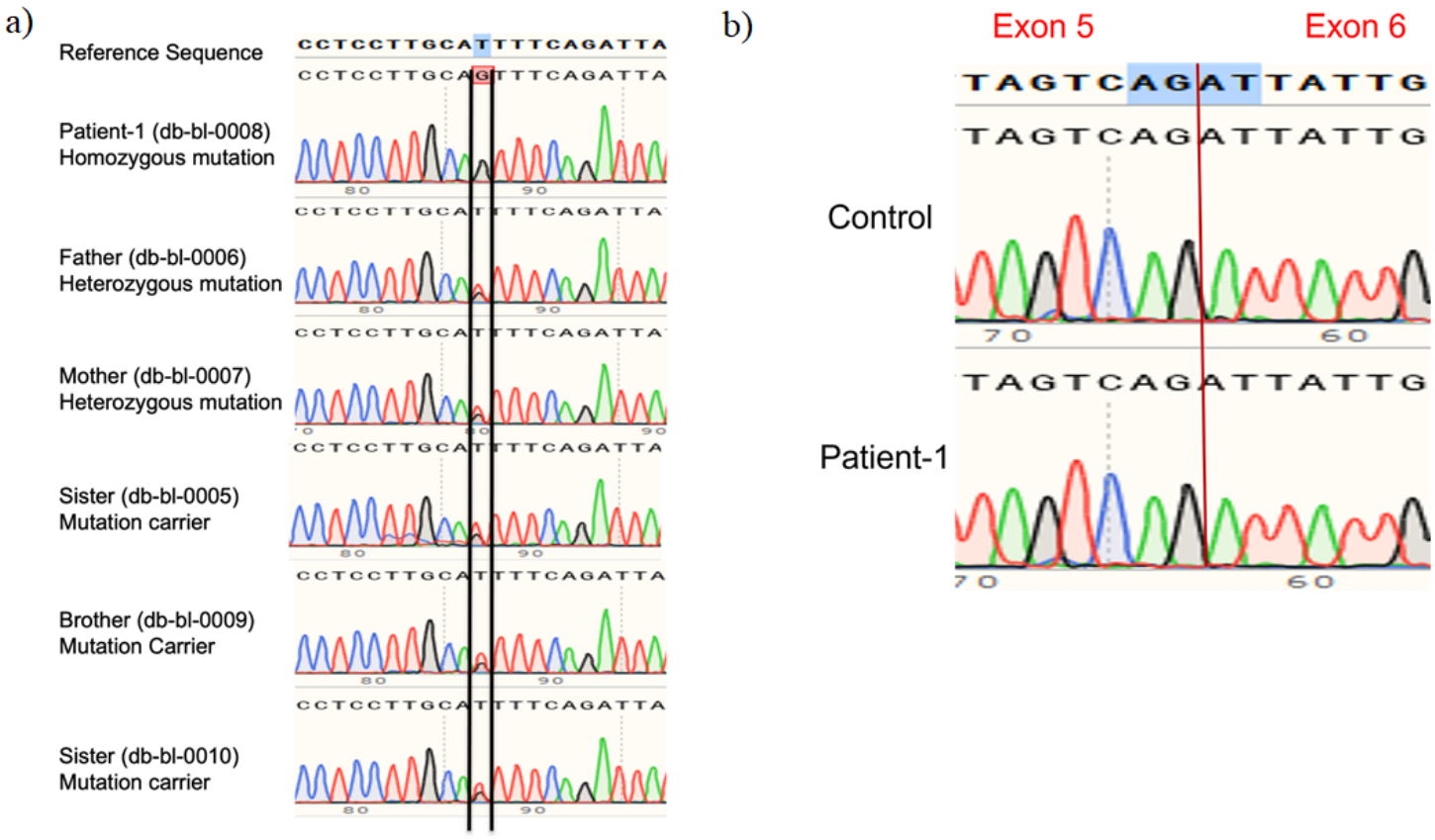

Figure 2

Genetic analysis for case 1 and family. (a) Sanger sequencing of DNA of the patient showed a novel homozygous mutation of *SLC2A2* (C. 613-7T>G, :IVS 5-7T>G) expected to effect a splice site between exons 5 and 6. (b) cDNA sequencing demonstrates that the splicing of exons 5 and 6 are unaffected by the intronic mutation. Parents are carriers of the mutation.

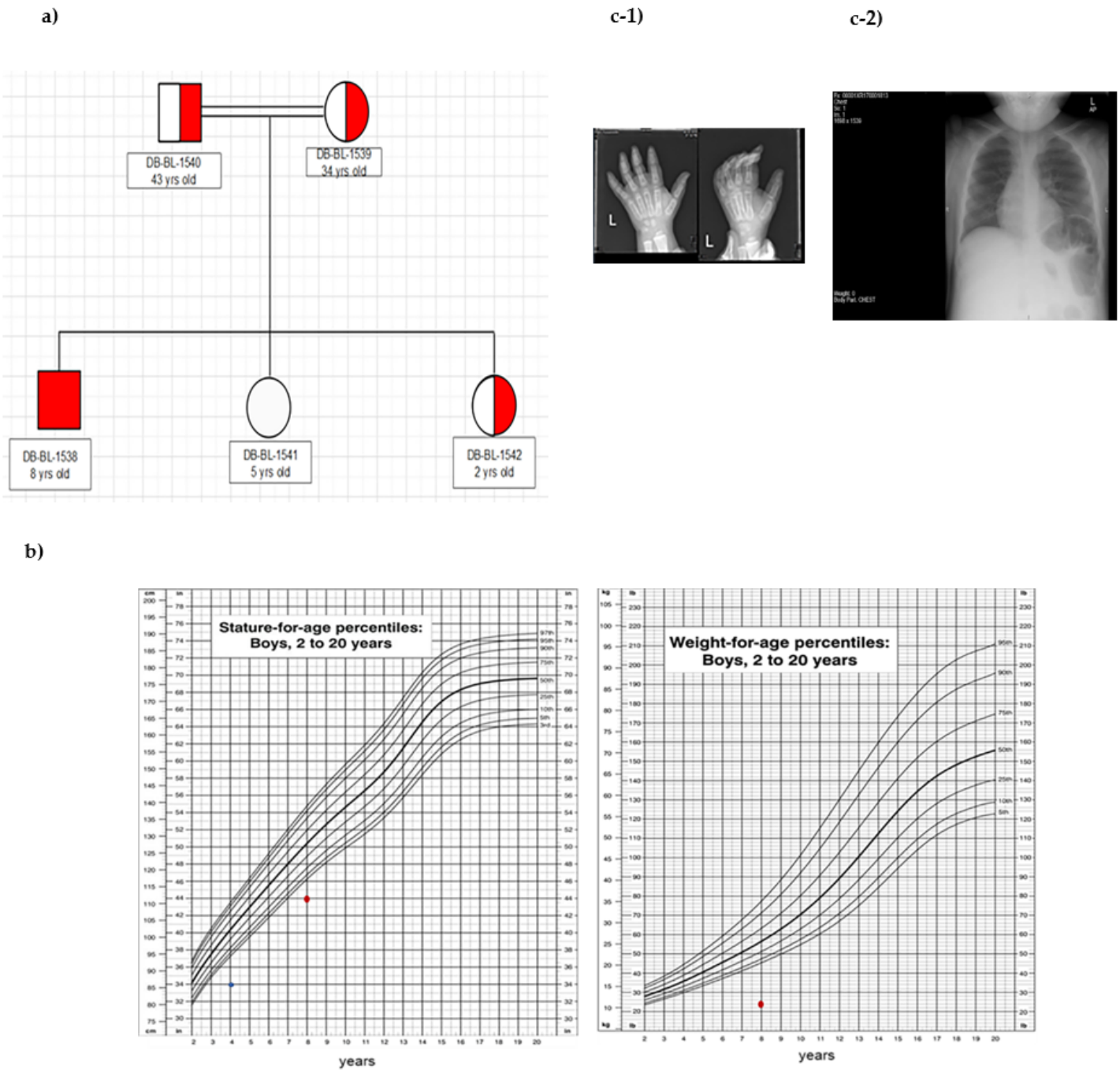

Figure 3

Clinical characteristics of case 2: (a) Family pedigree (patient descend from first-degree cousins). (b). Growth charts. According to CDC length chart, patient has short stature (dot), and underweight (dot). (c) Radiological findings, demonstrating the development of rickets (c-1), and hepatomegaly (c-2).

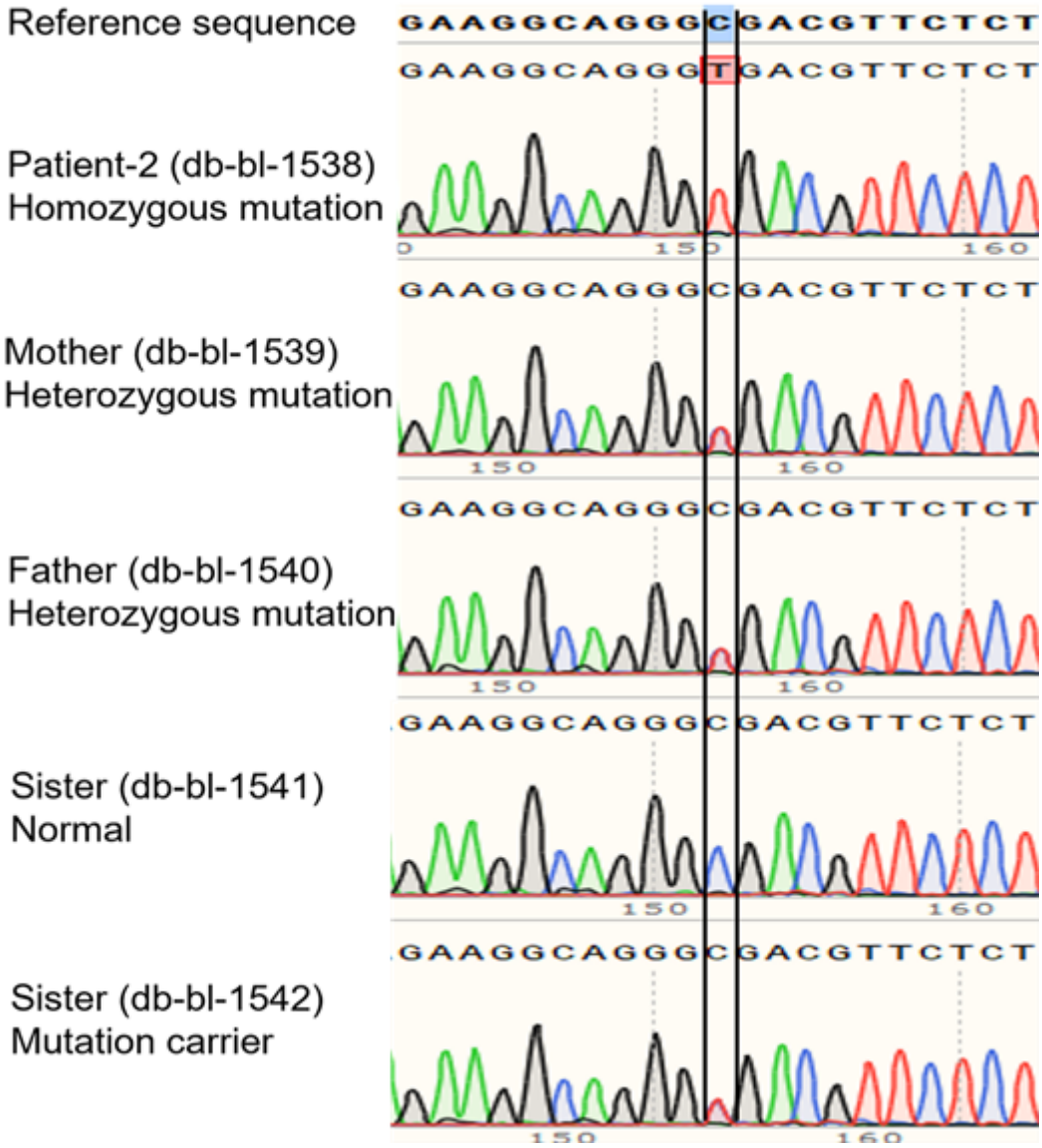

Figure 4

Genetic analysis for case 2 and family. Sanger sequencing of DNA showed a homozygous mutation of *SLC2A2* (c.1093C > T in exon 9, R365X) in the patient. Both parents are carriers of the mutation.

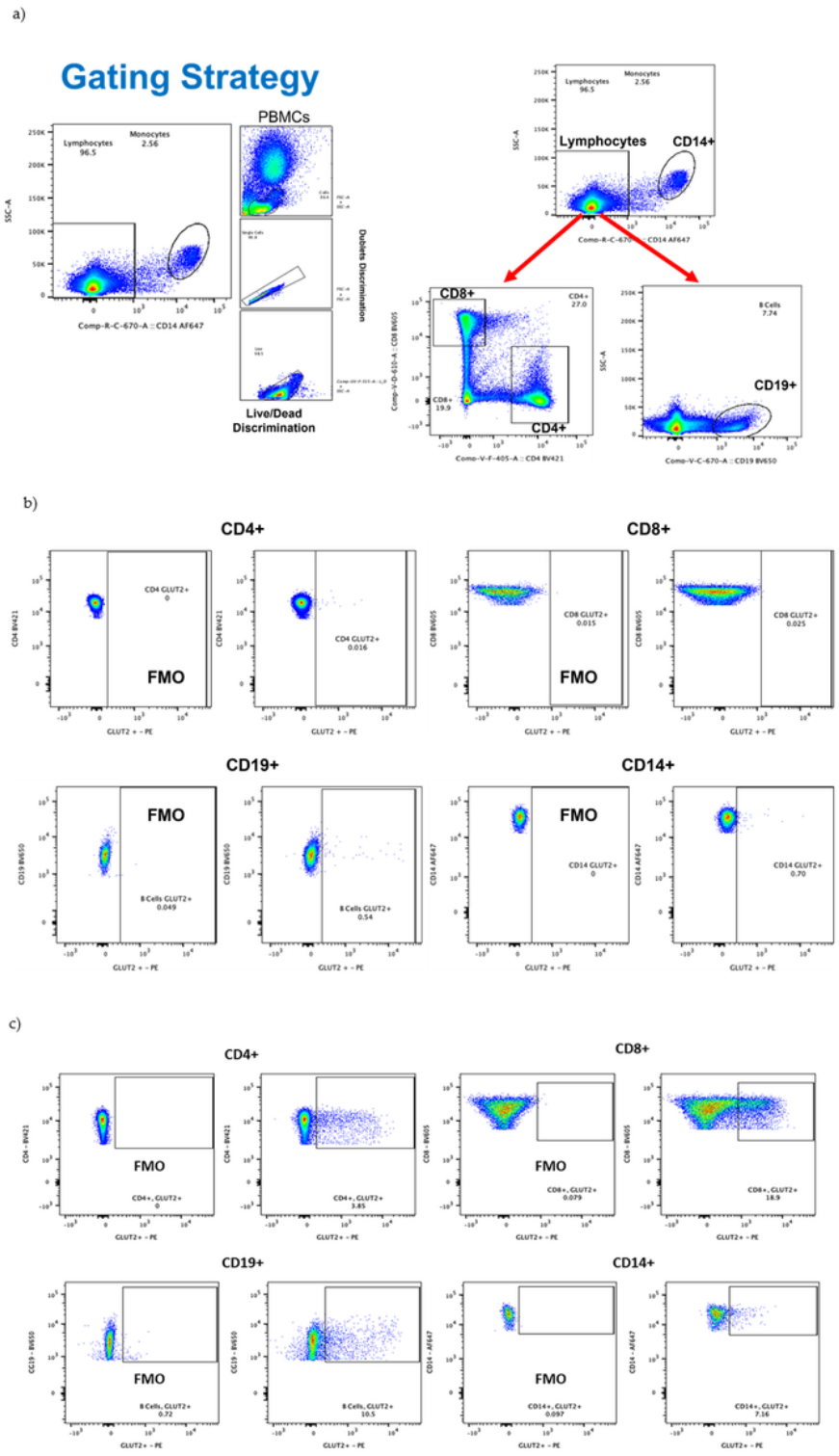

Figure 5

Flow cytometry to assess GLUT2 expression in each cell type in healthy PBMCs. (a) Illustration of the gating strategy used. T Lymphocytes (CD4+, CD8+), B lymphocytes (CD19+), monocytes (CD14+) extracted from a healthy control and the individual cells were sorted using the gate strategy illustrated in (a). (b) GLUT2 expression was very low in all cell population in PBMCs extracted from the healthy control.

(c) However, the expression of GLUT2 was increased in specific cell populations in PBMCs extracted from an immune-activated control.

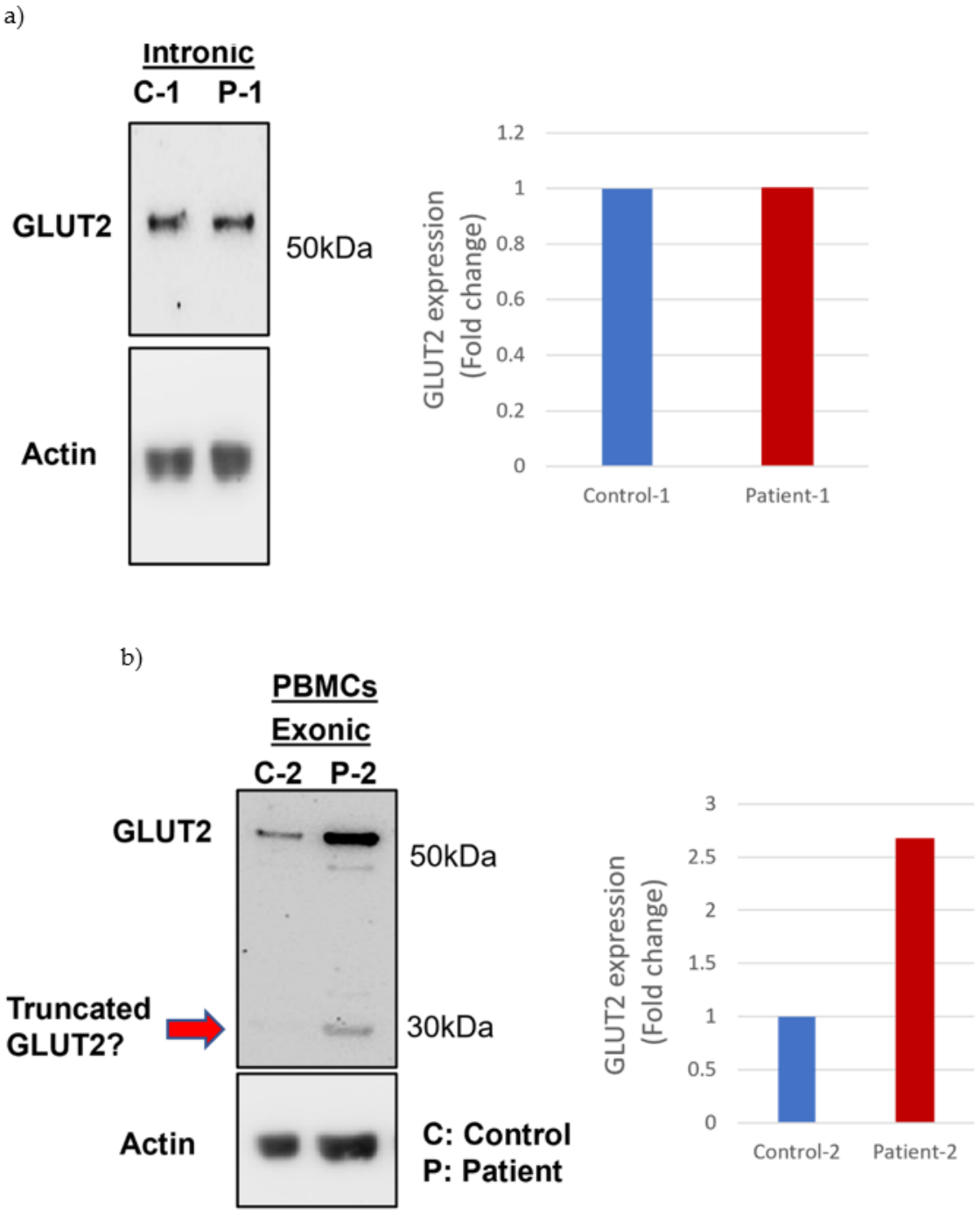

Figure 6

Western blotting to assess the expression of GLUT2 in patient and control PBMCs. (a) The expression of GLUT2 was similar in the patient with the intronic mutation in comparison to control. (b) The expression GLUT2 was increased in the patient with the exonic mutation. A smaller band was detected by the GLUT2 antibody in the sample obtained from the patient carrying the exonic mutation, indicated by the arrow. The quantification (fold-change) of GLUT2 in the samples are presented to the right in both (a) and (b).

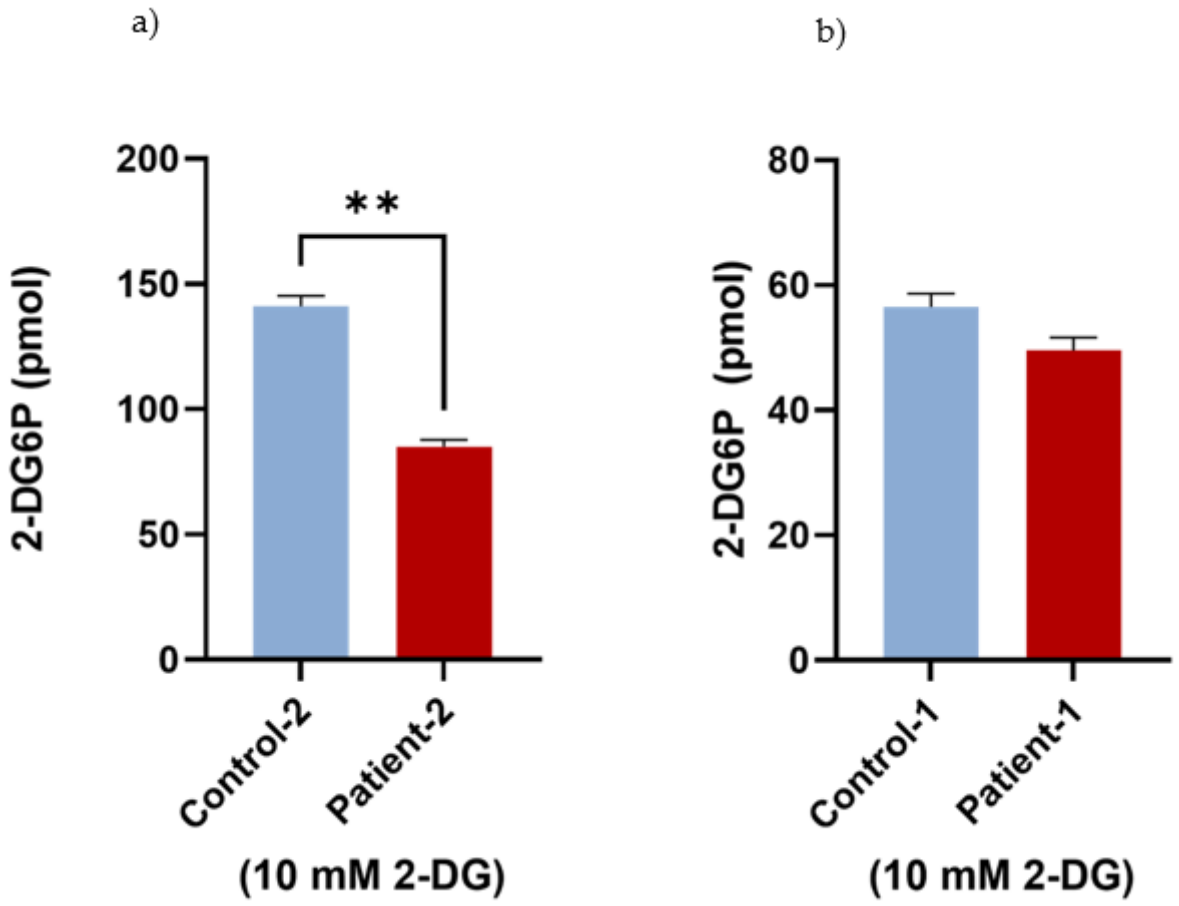

Figure 7

Glucose uptake test using patient PBMCs. (a) PBMCs from the patient with the exonic mutation had significantly decreased glucose uptake activity in comparison to control. (b) PBMCs from the patient with intronic mutation displayed the same glucose uptake activity as the control. P-value was calculated using two-tailed t-test and presented with a “*” in the graph. Error bar is the average reading of three independent experiments.

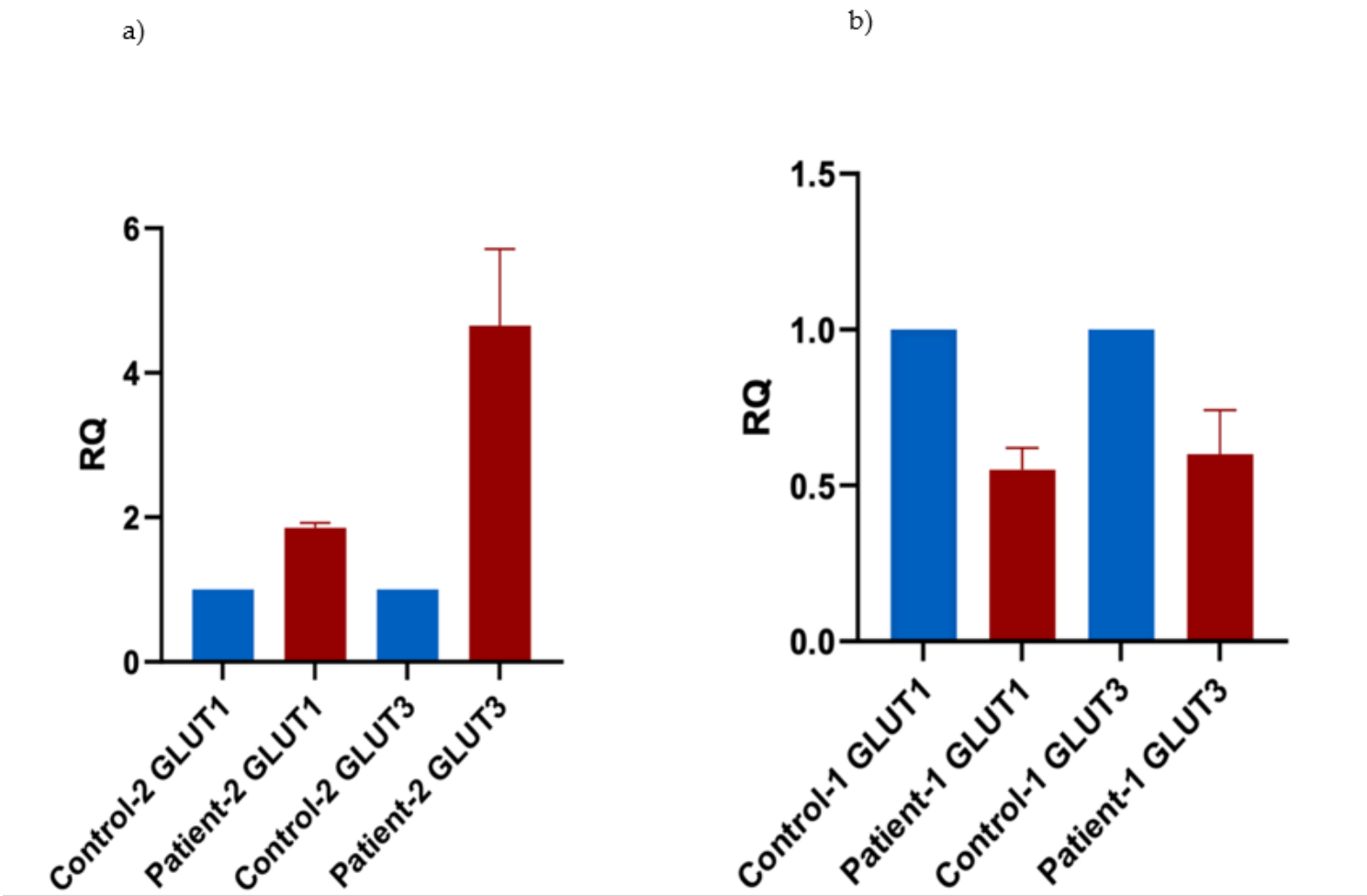

Figure 8

qRT-PCR to assess the expression of glucose transporters in patient PBMCs. (a) The mRNA levels of both GLUT1 and GLUT3 are elevated in PBMCs obtained from the patient carrying the exonic mutation. (b) In contrast, the mRNA levels of GLUT1 and GLUT3 are reduced in PBMCs obtained from the patient carrying the intronic GLUT2 mutation. Error bar is the average of technical replicates.

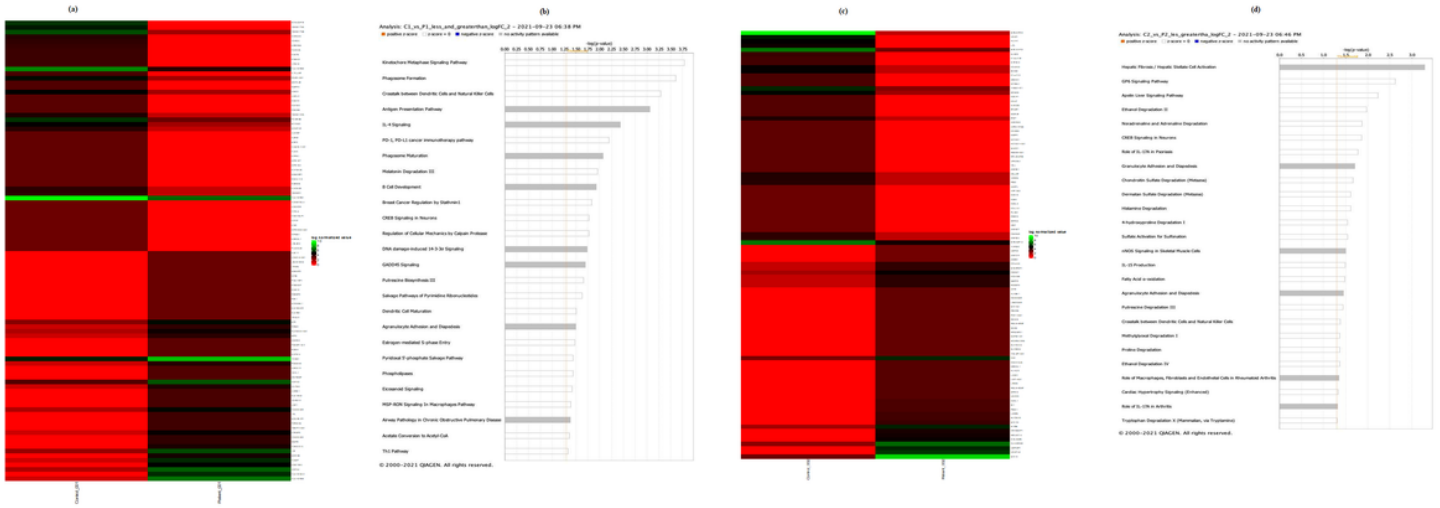

Figure 9

RNA-Seq analysis for patients and their controls. (a & c) Patients 1 and 2 had differentially regulated genes not associated with dysglycemia except for two genes (RETN (resistin) in patient-1 (found in >500 genes differentially regulated list) and ENPP1 in patient-2) involved in insulin resistance. (b & d) Pathways other than dysglycemia might be dysregulated in patients 1 and 2 in comparison to controls.

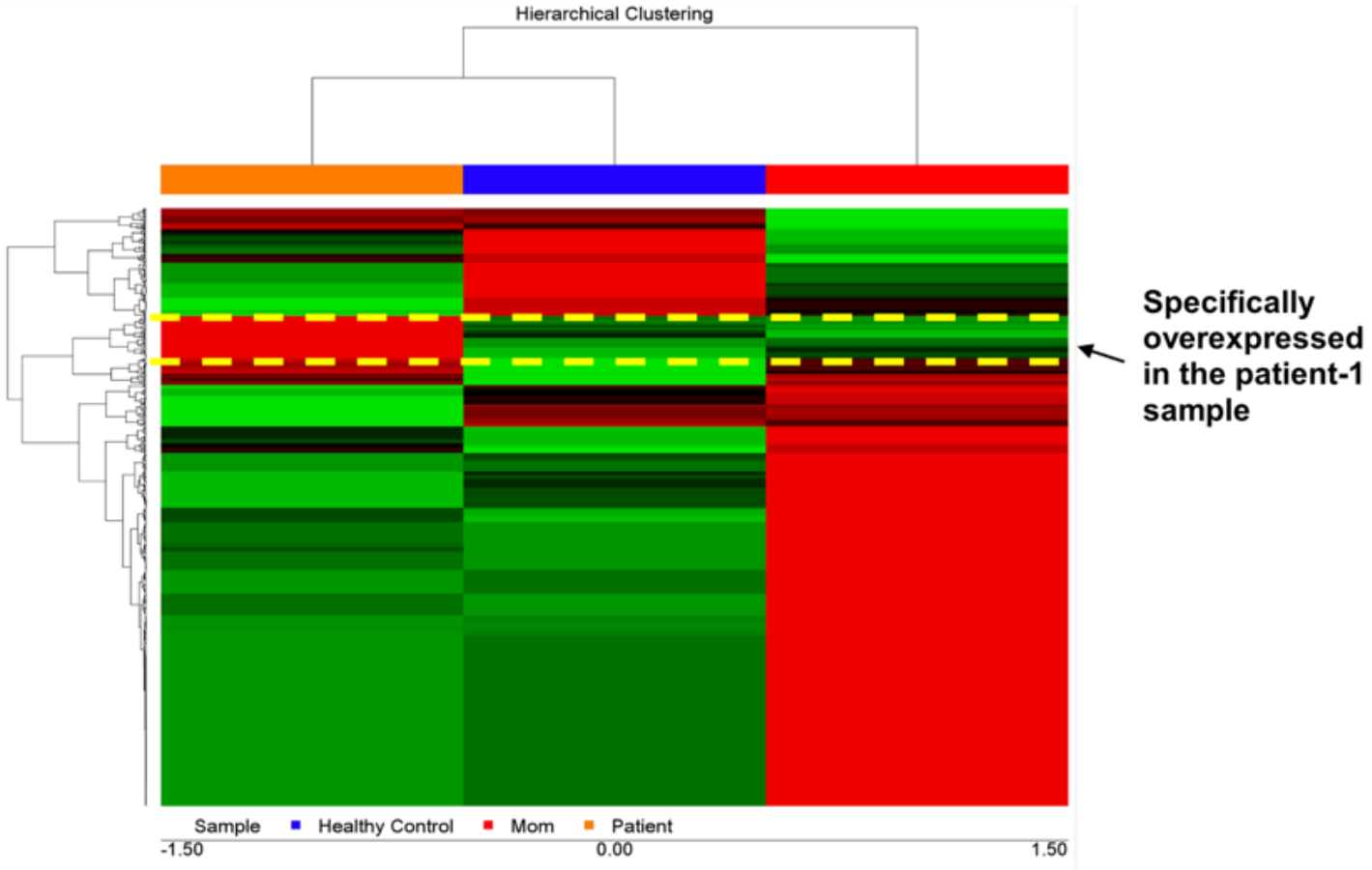

Figure 10

Heat map generated by Partek for case 1. 123 miRNAs were specific to the patient-1, with 118 mapped following IPA analysis. The region marked with the yellow dotted line includes miRNAs specially overexpressed in the patient.

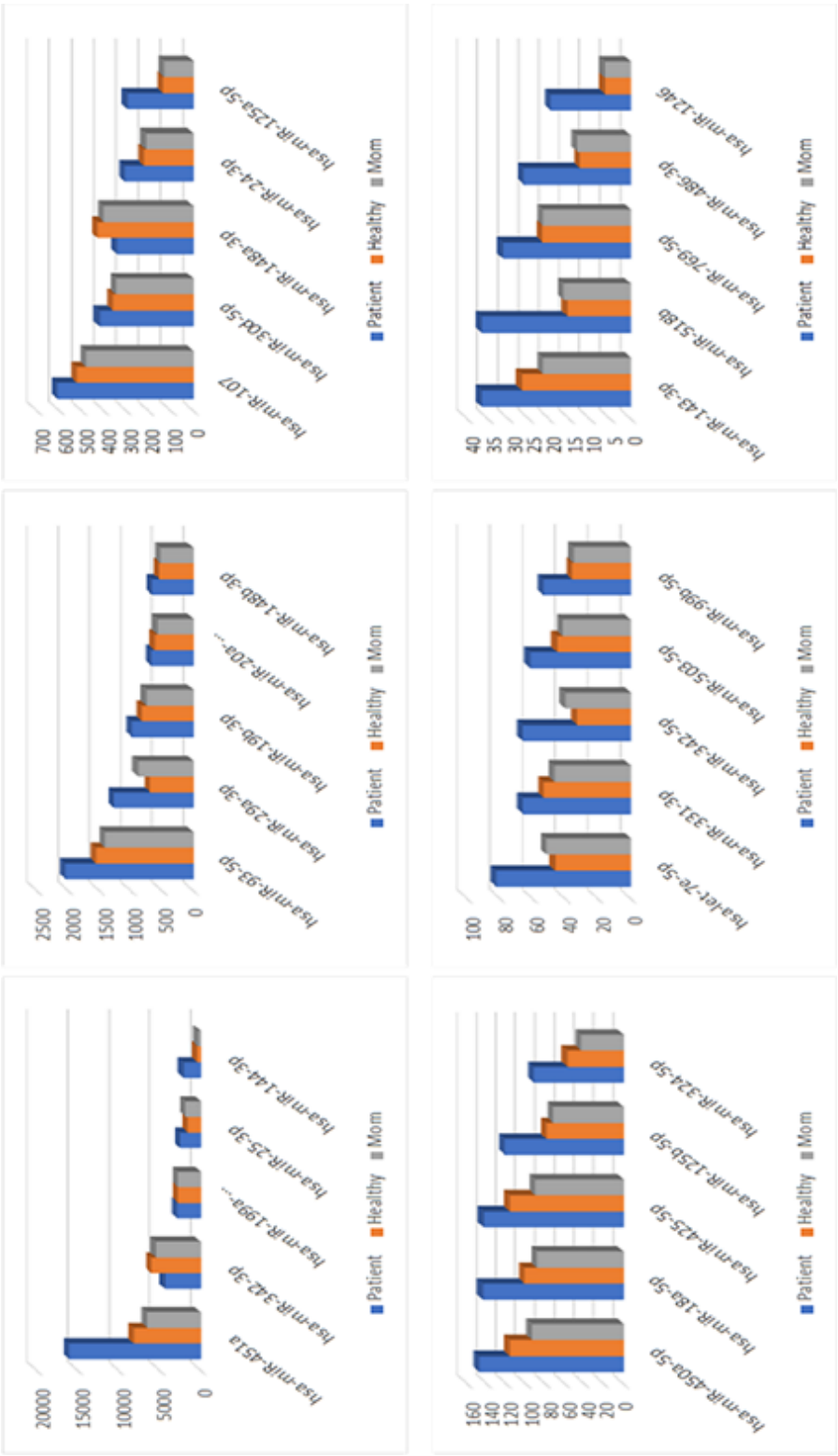

Figure 11

30 selected miRNAs with the highest number of counts difference in the patient with the intronic mutation in comparison to the healthy control. Fourteen miRNAs expressed in Type 1 diabetes mellitus were upregulated in the patient in comparison to control, and three of these (miR-144-3p, let-7e-5p, hsa-miR-29a-3p) were significantly overexpressed.

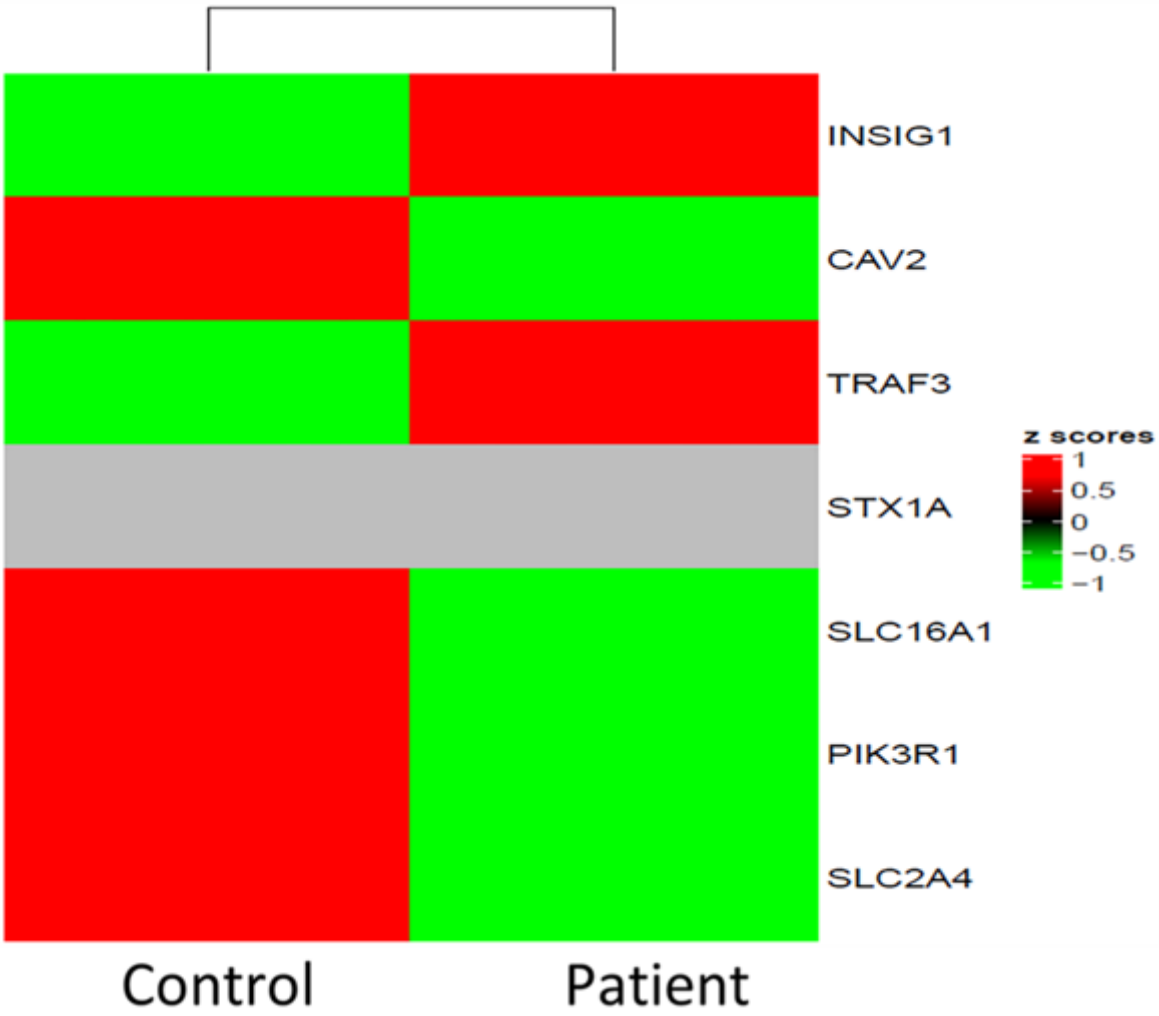

Figure 12

miR-29a-3b overexpression in the patient carrying the intronic GLUT2 mutation coincides with the downregulation of genes involved in insulin production and secretion. CAV2, SLC16A1, PIK3R1, and SLC2A4 were found to be downregulated in the patient in comparison to the healthy control.

Supplementary Files

This is a list of supplementary files associated with this preprint. Click to download.

- SupplementaryfiguresandtablesSanaaetal.ScRep.163.pdf